IEEE Access
Multidisciplinary | Rapid Review | Open Access Journal

Received July 25, 2021, accepted September 23, 2021, date of publication October 1, 2021, date of current version October 20, 2021.

Digital Object Identifier 10.1109/ACCESS.2021.3117079

A Weighting Radius Prediction Iteration Optimization Algorithm Used in Photogrammetry for Rotary Body Structure of Port Hoisting Machinery

ENSHUN LU[1], YANG LIU[2], ZHANGYAN ZHAO[3], YIFAN LIU[4], AND CHENGHUA ZHANG[3]

[1]School of Energy and Power Engineering, Wuhan University of Technology, Wuhan 430070, China
[2]School of Science, Wuhan University of Technology, Wuhan 430070, China
[3]School of Logistics Engineering, Wuhan University of Technology, Wuhan 430070, China
[4]China Harzone Industry Corporation Ltd., Wuhan 430200, China

Corresponding author: Yang Liu (yanglwhut@163.com)

This work was supported by the People's Republic of China Ministry of Science and Technology under Grant 2017YFC0805703.

ABSTRACT As a non-contact measurement technology with high data acquisition efficiency, photogrammetry is an ideal choice for collecting the data needed in the safety evaluation of port hoisting machinery. However, the radius fitting result accuracy cannot meet the requirements of safety assessment due to the limitation of the port crane itself and the working environment characteristics, when the existing photogrammetry method is used to measure the rotary body structure represented by the portal crane slewing mechanism. In order to solve this problem, an iterative optimization algorithm for weighted radius prediction for the photogrammetry of the slewing mechanism of port hoisting machinery is proposed in this paper. First, the algorithm uses the generalized multi-line rendezvous model to transform the radius fitting problem into the multi-line intersection point prediction problem, which lays a theoretical basis for the subsequent algorithm implementation. Second, by introducing a weighting algorithm based on the camera optical distortion model, the algorithm optimizes the accuracy of radius fitting results. In addition, through the quantitative evaluation method of fitting accuracy based on weighted algorithm, the algorithm also establishes a set of iterative rules to balance the accuracy of measurement results and the execution efficiency of the algorithm. Finally, this paper designs theoretical verification tests and simulation engineering tests based on the characteristics of the algorithm and the engineering practice of port hoisting machinery photogrammetry. The experimental results demonstrate that the algorithm described in this paper can significantly improve the accuracy of radius fitting results when the data quantity is small and the data quality is poor compared with the traditional algorithm.

INDEX TERMS Port hoisting machinery, rotary body structure, radius, weighting, iteration.

I. INTRODUCTION

Port hoisting machinery represented by quayside container crane, portal crane and gantry container crane is a kind of typical high-risk special equipment [1], [2]. Due to the frequent accidents and serious consequences, it is of great significance to study the safety monitoring methods for such equipment [3], [4].

As a non-contact measuring method with high data acquisition efficiency and excellent automation, photogrammetry is an ideal technical solution for port hoisting machinery safety monitoring. However, the application of photogrammetry in the field of port hoisting machinery safety monitoring has always been limited by the complex working environment of the port, which makes it impossible to get photos taken at reasonable distance and angle and with high background discrimination, resulting in unsatisfactory accuracy of measurement results calculated by traditional algorithm [5]–[7]. In order to solve this problem, the author

The associate editor coordinating the review of this manuscript and approving it for publication was Wuliang Yin.

and his team members put forward ''a weighted intersection point prediction algorithm for photogrammetry of port hoisting machinery'' based on the multi-line intersection points characteristics of key points of port hoisting machinery [8]. By weighting intersection lines based on optical distortion, the method realizes the principle of high-precision prediction of key points and significantly improves the measurement accuracy of key nodes of port hoisting machinery. However, the object of measurement in this method is box structure represented by front girder of quayside container crane and main girder of gantry container crane, which cannot serve the rotary body structure such as the column and slewing mechanism of the portal crane.

As a type of crane widely used in port frontline, it is of great significance to conduct safety research on portal crane [9]. This model is listed as one of the key research objects, in Key Technologies Research and Equipment Development for Risk Prevention and Control and Governance of Mechanical and Electrical Special Equipment (Project No. 2017YFC0805703), which is the national key R&D program of the Ministry of Technology of the People's Republic of China. In order to achieve high-precision photogrammetry of portal crane, this paper has carried out research on the optimization method of photogrammetric accuracy of revolving body structure, and proposed ''an iterative optimization algorithm for weighted radius prediction for photogrammetry of port hoisting machinery slewing structure''.

By utilizing the feature that the perpendicular lines intersect at the center of the circle in the chordae of the circle, the roundness error caused by the measurement error at each point of the circle during the actual measurement is converted into a non-strict intersection of the mid-perpendicular lines, so that the measuring accuracy of the radius calculated by adjustment of the circle center coordinate and the circle center coordinate can be optimized by the multi-line intersection point prediction model.

The algorithm uses the characteristic that the perpendicular bisector of each chord around the circle intersects at the center of the circle, and converts the roundness error caused by the measurement error of each point of the circle in the actual measurement process into the non-strict intersection of the mid-vertical line. This paper optimizes the circle center coordinates through the multi-line intersection point prediction model and the measurement accuracy of the radius obtained by the adjustment calculation based on the circle center coordinates [8].On this basis, considering the different measurement errors caused by optical distortion at each point of the image plane, a weighted model for predicting and calculating the multi-line intersection point at the center of the circle is proposed, which realizes the quantitative description of the error introduced by optical distortion and further improves the measurement accuracy. Finally, the algorithm establishes a set of iteration rules based on the quantitative evaluation method of the fitting accuracy of weighted algorithm, which realizes the balance between the precision of measurement results and the execution efficiency of the algorithm.

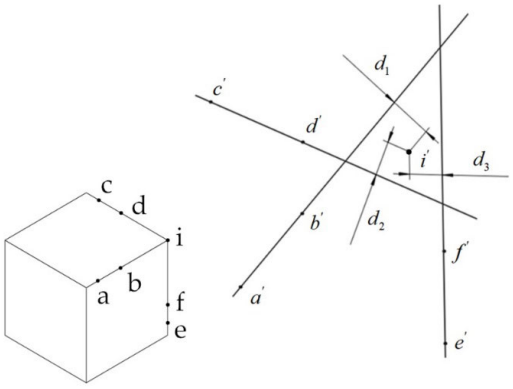

FIGURE 1. Schematic diagram of multi-line intersection principle.

The rest of this paper is arranged as follows: Section II describes the details of the algorithm and the implementation process. In the third section, according to the characteristics of the algorithm, indoor and outdoor experiments are set up, corresponding to the cylinder model and the portal crane model, respectively. The test results in Section III are analyzed and discussed in Section IV. Finally, in Section V, the conclusions and prospects of this paper are given.

II. METHODOLOGY

A. GENERALIZED MULTILINE INTERSECTION PRINCIPLE

As shown in Fig. 1, in the paper ''A weighting intersection point prediction iteration optimization algorithm used in photogrammetry for port hoisting mechanism'' published by the author before, point i is taken as an example to show that the key joint of port hoisting machinery structure belongs to the characteristics of multi-line intersection point. The straight line l_{ab}, l_{cd}, l_{ef} determined by points a, b, c, d, e and f are introduced as the positioning basis of point i, and the phenomenon that the spatial straight lines $l_{a'b'}$, $l_{c'd'}$, $l_{e'f'}$ restored by the actual measurement results cannot meet at the same point due to the existence of errors are used. By weighting the distance d_1, d_2, d_3 from the predicted intersection point i (TPPOI) to each intersection line in the solution model (TEWIPPA), the quantified weighting of the observed data is realized based on the size of the theoretical optical distortion of each point while introducing redundant observation data, and a relatively ideal precision optimization effect is obtained [8].

However, this method does not apply to the safety evaluation research of the rotary body structure represented by the slewing mechanism of portal crane as shown in Fig. 2, because this method requires the measured object to have a regular shape with obvious edge line characteristics. In order to introduce redundant observation data and improve measurement accuracy by weighted adjustment operation, the measuring principle shown in Fig. 3 is adopted in this paper,

FIGURE 2. Schematic diagram of slewing mechanism.

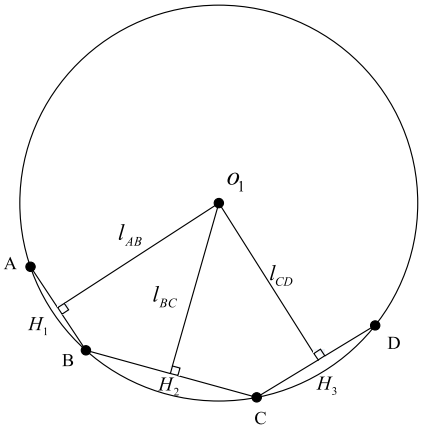

FIGURE 3. Fitting principle of circle center and radius.

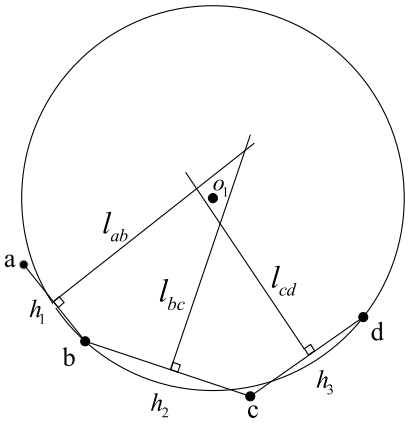

FIGURE 4. The intersection of perpendiculars during the actual measurement.

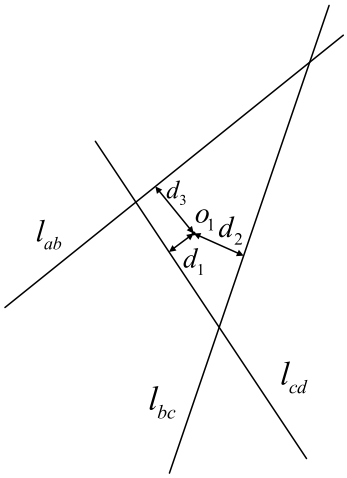

FIGURE 5. Schematic diagram of circle center prediction principle.

which transforms the rotary body structure into a generalized multi-line intersection structure.

The main data to be obtained by measuring the rotary body structure are the coordinates of the center of the circle of each circular section and the corresponding radius parameters of the section. As shown in Fig. 3, based on the principle that the perpendicular bisector of any two points on a circle must pass through the center of the circle, by measuring the points A, B, C, and D on the same circle section, the position of the center point O can be determined according to the intersection of the vertical lines l_{AB}, l_{BC}, l_{CD}, and the radius can be calculated. Therefore, when the radius parameters are measured, the rotary body can also be regarded as a generalized multi-line intersection structure.

B. EQUAL WEIGHT RADIUS PREDICTION OF ROTARY BODY STRUCTURE

The measurement method described in Section generalized multiline intersection principle is based on the geometric feature that the perpendicular bisector of each pair of feature points must pass through the center of the circle. However, due to inevitable measurement errors, the perfect intersection of the perpendicular bisector shown in Fig. 3 at the same point will hardly occur in the actual measurement process, but will appear as a non-strict intersection state as shown in Fig. 4.

As shown in Fig. 4, point a, point b, point c and point d are respectively object points restored from the measured values of point A, point B, point C and point D in Fig. 3 and the perpendicular bisector l_{ab}, l_{bc}, l_{cd} of them cannot intersect at the same point due to the existence of measurement errors. Therefore, according to the idea of establishing the predictive intersection point solution model (TEWIPPA) [8], the center O can be obtained according to the principle shown in Fig. 5 in the actual measurement the principle shown in Fig. 5 in the actual measurement process. Find the minimum point o of the distance d_1, d_2, d_3 sum of three straight lines l_{ab}, l_{bc}, l_{cd} in object square space, and use point o as the prediction point of the circle center O. Because d_1, d_2, d_3 can be used to measure the confidence level of the perpendicular bisector l_{ab}, l_{bc}, l_{cd} [10], weighted adjustment can be carried out based on d_1, d_2, d_3 to improve the accuracy

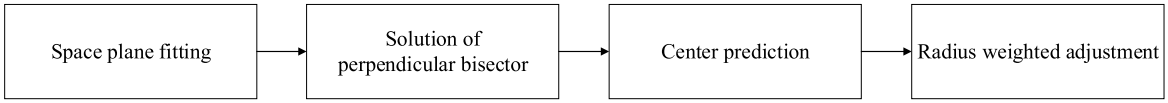

FIGURE 6. Prediction algorithm of equal weight rotary radius.

of measurement results, in the process of radius fitting. Since the prediction of point O is based on the same confidence of straight lines, we call this algorithm prediction algorithm of equal weight rotary body. The flow of the algorithm is as follows:

In order to ensure the execution efficiency of the algorithm, the algorithm described in this paper only uses the perpendicular bisector between adjacent points for solution. Details of the prediction algorithm of equal weight rotary radius are as follows.

1) SPACE PLANE FITTING ALGORITHM

Set: The object square coordinates of each characteristic point used to fit the center and radius of the circle are respectively: (X_{Wi}, Y_{Wi}, Z_{Wi}), where i is the number of characteristic points. In subsequent sections of the paper, we call them fitting points. In order to facilitate the solution, let the space plane equation fitted by each feature point be $A \cdot X + B \cdot Y + C \cdot Z + D = 0$, then according to the coplanar constraint condition, formula 1 can be obtained as shown at the bottom of the page.

According to this formula, the solution of space plane equation $A \cdot X + B \cdot Y + C \cdot Z + D = 0$ can be completed.

2) ALGORITHM FOR SOLVING PERPENDICULAR BISECTOR

In the traditional space circle fitting algorithm, after completing the fitting of the space plane where each point is used for the solution, the spherical equation $(X-a)^2+(Y-b)^2+(Z-c)^2-R^2=0$ with the equal radius of the space circle and the center O as the spherical center needs to be solved according to the distance constraints, as shown in formula 2 as shown at the bottom of the page.

The expression of the space circle can be obtained by simultaneous solution of spherical equation $(X-a)^2+(Y-b)^2+(Z-c)^2-R^2=0$ and space plane equation $A \cdot X + B \cdot Y + C \cdot Z + D = 0$ from formula 1.

Since only simple data fitting is used, a large number of space point data is required to ensure the accuracy of traditional algorithm. In the slewing mechanism of port hoisting machinery, the cross-section between slewing mechanism and other structures is usually selected for measuring the radius of section, but such interface is generally higher off the ground and there are no climbing facilities around it.

Therefore, due to safety considerations, it is difficult to set manual measuring marks on the surface of the measured object according to the traditional photogrammetric

$$\begin{bmatrix} \frac{A}{D} \\ \frac{B}{D} \\ \frac{C}{D} \end{bmatrix} = \begin{bmatrix} -\sum_{k=1}^{i} X_{Wk}^2 & -\sum_{k=1}^{i} X_{Wk} \cdot Y_{Wk} & -\sum_{k=1}^{i} X_{Wk} \cdot Z_{Wk} \\ -\sum_{k=1}^{i} X_{Wk} \cdot Y_{Wk} & -\sum_{k=1}^{i} Y_{Wk}^2 & -\sum_{k=1}^{i} Y_{Wk} \cdot X_{Wk} \\ -\sum_{k=1}^{i} X_{Wk} \cdot Z_{Wk} & -\sum_{k=1}^{i} Y_{Wk} \cdot Z_{Wk} & -\sum_{k=1}^{i} Z_{Wk}^2 \end{bmatrix} \cdot \begin{bmatrix} -\sum_{k=1}^{i} X_{Wk} \\ -\sum_{k=1}^{i} Y_{Wk} \\ -\sum_{k=1}^{i} Z_{Wk} \end{bmatrix}. \tag{1}$$

$$\begin{bmatrix} 2a \\ 2b \\ 2c \\ a^2+b^2+c^2-R^2 \end{bmatrix} = \begin{bmatrix} -\sum_{k=1}^{i} X_{Wk}^2 & -\sum_{k=1}^{i} X_{Wk} \cdot Y_{Wk} & -\sum_{k=1}^{i} X_{Wk} \cdot Z_{Wk} & -\sum_{k=1}^{i} X_{Wk} \\ -\sum_{k=1}^{i} X_{Wk} \cdot Y_{Wk} & -\sum_{k=1}^{i} Y_{Wk}^2 & -\sum_{k=1}^{i} Y_{Wk} \cdot X_{Wk} & -\sum_{k=1}^{i} Y_{Wk} \\ -\sum_{k=1}^{i} X_{Wk} \cdot Z_{Wk} & -\sum_{k=1}^{i} Y_{Wk} \cdot Z_{Wk} & -\sum_{k=1}^{i} Z_{Wk}^2 & -\sum_{k=1}^{i} Z_{Wk} \\ -\sum_{k=1}^{i} X_{Wk} & -\sum_{k=1}^{i} Y_{Wk} & -\sum_{k=1}^{i} Z_{W_k} & i \end{bmatrix} \cdot \begin{bmatrix} \sum_{k=1}^{i} X_{Wk} \cdot \left(X_{Wk}^2 + Y_{Wk}^2 + Z_{Wk}^2\right) \\ \sum_{k=1}^{i} Y_{Wk} \cdot \left(X_{Wk}^2 + Y_{Wk}^2 + Z_{Wk}^2\right) \\ \sum_{k=1}^{i} Z_{Wk} \cdot \left(X_{Wk}^2 + Y_{Wk}^2 + Z_{Wk}^2\right) \\ \sum_{k=1}^{i} \left(X_{Wk}^2 + Y_{Wk}^2 + Z_{Wk}^2\right) \end{bmatrix}. \tag{2}$$

method in the actual operation of port hoisting machinery photogrammetric work. The measurement can only be carried out according to the characteristic points of the port hoisting machinery itself represented by the intersection of stiffener and slewing mechanism boundary. This method makes the number of measuring points extremely limited, often no more than 10, which results in that the solution accuracy of traditional algorithm is difficult to meet the requirements of port hoisting machinery measurement work.

In order to improve the accuracy of the measurement results as much as possible, the spatial circle fitting of the algorithm described in this section is based on the principle of intersection point of the perpendicular bisector. Solving the expression of the perpendicular bisector connecting each object point of the fitting circle is the basis of this method. Taking the solution of the perpendicular bisector l_{ab} in Fig. 4 as an example, the solution algorithm used in this paper is as follows:

Set: The parametric equation of the perpendicular bisector l_{ab} is $\frac{X-X_A}{m}+\frac{Y-Y_A}{n}+\frac{Z-Z_A}{p}=t$; The coordinate of the object space of point a and point b are (X_a, Y_a, Z_a) and (X_b, Y_b, Z_b).

Since the point h_1, which is the plumb foot of the perpendicular bisector, is theoretically very close to the spatial plane fitted by the algorithm described in Section space plane fitting algorithm, it can be approximately considered that the point is above the plane. According to the characteristic that the straight line l_{ab} is perpendicular to the line connecting points a and b and the straight line l_{ab} is located on the fitting space plane, the parameters in the l_{ab} straight line equation should satisfy the following conditions:

$$\begin{bmatrix} m & n & p \end{bmatrix} = \begin{bmatrix} X_A - X_B & Y_A - Y_B & Z_A - Z_B \end{bmatrix} \otimes \begin{bmatrix} \frac{X_A + X_B}{2} & \frac{Y_A + Y_B}{2} & \frac{Z_A + Z_B}{2} \end{bmatrix} \quad (3)$$

According to formula 3, the values of m, n and p can be solved.

3) CIRCLE CENTER PREDICTION ALGORITHM

To carry out the forecasting calculation of the center of circle, the distance between the center of circle and the perpendicular bisector must be calculated. We named this calculation model as the circle center - vertical foot distance solution model.

Definition 1: Circle center-vertical foot distance solution model (DYD)

Set: The object square coordinate of the center of a circle is (X_o, Y_o, Z_o); The relevant parameters of each perpendicular bisector equation calculated by the algorithm described in Section algorithm for solving perpendicular bisector are m_g, n_g, p_g, where $g = 1, 2, \ldots, i-1$; And the object square coordinates of the fitting points corresponding to each perpendicular bisector are (X_g, Y_g, Z_g), $(X_{g+1}, Y_{g+1}, Z_{g+1})$.

According to the solution formula of distance from the space point to the straight line, the circle center-vertical foot distance solution model (DYD) is shown in formula 4, as shown at the bottom of the page.

The (X_o, Y_o, Z_o) corresponding to the minimum value $DYD_{\min}$ of formula 4 is the prediction result of the center of circle. We call this point in the object square coordinate system equal weight forecasting center O_m.

4) RADIUS WEIGHTED ADJUSTMENT ALGORITHM

Due to the existence of measurement error, the distance between the equal weight prediction center o_m and each fitting point, that is, the corresponding solution radius of each fitting point, is not the same. In order to increase the accuracy of radius measurement results as much as possible, it is necessary to adjust these data.

Since the measurement errors of each fitting point must be different, it is obviously unreasonable to simply average the calculated radius corresponding to each fitting point. As mentioned above, the distance dd_g between the center o_m of the equal weight forecast and the perpendicular bisector is inversely proportional to the reliability of the fitting point corresponding to the perpendicular bisector. Therefore, dd_g can be used as a quantitative evaluation standard for the confidence level of the solution radius corresponding to each fitting point. According to the circle center-vertical foot distance solution model, the calculation formula of dd_m is as follows (5), shown at the bottom of the next page.

After normalization, the corresponding solution radius of the fitting points constituting each perpendicular bisector in the weighted adjustment algorithm corresponds to the weight QO_g.

According to the weight calculation method described in formula 6, as shown at the bottom of the next page, the weight adjustment algorithm formula of radius of rotary

$$DYD = \sum_{g=1}^{i-1} \left\{ \begin{array}{l} \left\{ X_o - \left[m_g \cdot \dfrac{m_g \cdot (X_o - X_g) + n_g \cdot (Y_o - Y_g) + p_g \cdot (Z_o - Z_g)}{m_g^2 + n_g^2 + {p_g}^2} + X_g \right] \right\}^2 \\ + \left\{ Y_o - \left[n_g \cdot \dfrac{m_g \cdot (X_o - X_g) + n_g \cdot (Y_o - Y_g) + p_g \cdot (Z_o - Z_g)}{m_g^2 + n_g^2 + p_g^2} + Y_g \right] \right\}^2 \\ + \left\{ Z_o - \left[p_g \cdot \dfrac{m_g \cdot (X_o - X_g) + n_g \cdot (Y_o - Y_g) + p_g \cdot (Z_o - Z_g)}{m_g^2 + n_g^2 + p_g^2} + Z_g \right] \right\}^2 \end{array} \right\}^{\frac{1}{2}} \quad (4)$$

body is shown in formula 7, as shown at the bottom of the page.

It can be seen from definition 1 that the circle center-vertical foot distance solution model (DYD) is established based on the fact that the perpendicular bisector involved in the center prediction have the same weight coefficient.

Therefore, the algorithm described in this section is called equal weight radius prediction of rotary body structure.

C. WEIGHTED RADIUS PREDICTION OF ROTARY BODY STRUCTURE

1) WEIGHTED RADIUS PREDICTION OF ROTARY BODY STRUCTURE

The fitting points are used to determine each perpendicular bisector in the actual measurement process, but the measurement errors contained in the fitting points are different. Therefore, there is still room for improvement in the accuracy of the center of circle predicted according to the circle center-vertical foot distance solution model adopted by equal weight radius prediction algorithm of rotary body structure.

In order to give a more objective and scientific description of the intersection of each perpendicular bisector in the actual measurement process, so as to improve the accuracy of the prediction results of the center of circle, the weighted radius prediction algorithm of the rotary body structure described in this section improves the circle center-vertical foot distance solution model (DYD), and a weighted circle center-vertical foot distance solution model (QDYD) is formed.

Definition 2: Weighted circle center-vertical foot distance solution model (QDYD).

Set: The weight corresponding to each perpendicular bisector in the solution model is QL_g, then the weighted circle center-vertical foot distance solution model (QDYD) is shown in formula 8, as shown at the bottom of the next page.

In formula 8, the weight coefficients of each perpendicular bisector are calculated as follows.

2) QDYD CALCULATION METHOD OF WEIGHT COEFFICIENT

The same idea as the weighting algorithm described in the paper "A weighting intersection point prediction iteration optimization algorithm used in photogrammetry for port hoisting machinery" [8] the measurement errors at each fitting point can be quantitatively evaluated based on the camera optical distortion model.

$$dd_g = \left\{ \begin{array}{l} \left\{ X_0 - \left[m_g \cdot \dfrac{m_g \cdot (X_0 - X_g) + n_g \cdot (Y_0 - Y_g) + p_g \cdot (Z_o - Z_g)}{m_g^2 + n_g^2 + p_g^2} + X_g \right] \right\}^2 \\ + \left\{ Y_o - \left[n_g \cdot \dfrac{m_g \cdot (X_0 - X_g) + n_g \cdot (Y_o - Y_g) + p_g \cdot (Z_o - Z_g)}{m_g^2 + n_g^2 + p_g{}^2} + Y_g \right] \right\}^2 \\ + \left\{ Z_0 - \left[p_g \cdot \dfrac{m_g \cdot (X_0 - X_g) + n_g \cdot (Y_0 - Y_g) + p_g \cdot (Z_0 - Z_g)}{m_g^2 + n_g^2 + p_g^2} + Z_g \right] \right\}^2 \end{array} \right\}^{\frac{1}{2}} \tag{5}$$

$$QO_g = \frac{\left(\begin{array}{l} \left\{ X_o - \left[m_g \cdot \frac{m_g \cdot (X_o - X_g) + n_g \cdot (Y_o - Y_g) + p_g \cdot (Z_o - Z_g)}{m_g^2 + n_g^2 + p_g^2} + X_g \right] \right\}^2 \\ + \left\{ Y_o - \left[n_g \cdot \frac{m_g \cdot (X_o - X_g) + n_g \cdot (Y_o - Y_g) + p_g \cdot (Z_o - Z_g)}{m_g^2 + n_g^2 + p_g^2} + Y_g \right] \right\}^2 \\ + \left\{ Z_o - \left[p_g \cdot \frac{|n_g \cdot (X_o - X_g) + n_g \cdot (Y_o - Y_g) + p_g \cdot (Z_o - Z_g)}{m_g^2 + n_g^2 + p_g^2} + Z_g \right] \right\}^2 \end{array} \right)^{\frac{1}{2}}}{\sum_{g=1}^{i-1} \left(\begin{array}{l} \left\{ X_o - \left[m_g \cdot \frac{m_g \cdot (X_o - X_g) + n_g \cdot (Y_o - Y_g) + p_g \cdot (Z_o - Z_g)}{m_g^2 + n_g^2 + p_g^2} + X_g \right] \right\}^2 \\ + \left\{ Y_o - \left[n_g \cdot \frac{m_g \cdot (X_o - X_g) + n_g \cdot (Y_o - Y_g) + p_g \cdot (Z_o - Z_g)}{m_g^2 + n_g^2 + p_g^2} + Y_g \right] \right\}^2 \\ + \left\{ Z_o - \left[p_g \cdot \frac{m_g \cdot (X_o - X_g) + n_g \cdot (Y_o - Y_g) + p_g \cdot (Z_o - Z_g)}{m_g^2 + n_g^2 + p_g^2} + Z_g \right] \right\}^2 \end{array} \right)^{\frac{1}{2}}} \tag{6}$$

$$R_{DQ} = \sum_{g=1}^{i-1} QO_g \cdot \frac{\sqrt{(X_0 - X_g)^2 + (Y_0 - Y_g)^2 + (Z_0 - Z_g)^2} + \sqrt{(X_0 - X_{g+1})^2 + (Y_0 - Y_{g+1})^2 + (Z_0 - Z_{g+1})^2}}{2} \tag{7}$$

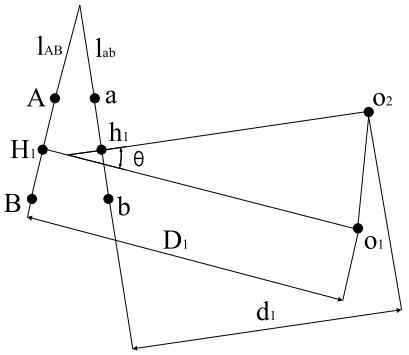

FIGURE 7. Schematic diagram of calculation model for weight coefficient QDYD.

The distance between the center of circle predicted by fitting points and the true center of circle can intuitively reflect the errors contained in the prediction results, and it is the best scale for calculation QL_g. In this section, we will discuss the distance between the predicted center based on the optical distortion model and the real center, and on this basis, we will calculate the method of QL_g.

Since optical distortion model is used as the calculation datum of weighting coefficient, the calculation method of weighting coefficient QDYD is carried out in each phase plane coordinate system. The principle of this method is shown in Fig. 7, taking the calculation process of the weight coefficient of the perpendicular bisector l_{AB} in Fig. 3 as an example.

Fig. 7 shows the image plane coordinate system of a certain measurement photograph, in this coordinate system: Points A and B are theoretical image points which do not include optical distortion error in the image plane; Points a and b are true image points containing optical distortion errors; Point o_1 is the theoretical image points of the center coordinate and point o_2 is the real image point containing optical distortion. Point o_1 and point o_2, as mentioned above, are not real image points, in which point o_2 is the equal weight forecasting center calculated by the algorithm described in Section weighted radius prediction of rotary body structure. Points H_1 o_1 and H_2 are the projection points of the vertical foot of the perpendicular bisector in space. According to the principle of invariant projection geometry proportion, they are the midpoints of the connecting lines of point A and Point B and the connecting lines of point a and point b respectively.

Set: the square coordinate of point o_2 to (X_{o2}, Y_{o2}, Z_{o2}).

According to the projection formula of space point and image point, the image plane coordinate (x_{o2}, y_{o2}) of point o_2 can be obtained, as shown in formula 9.

$$\begin{cases} x_{02} = -f \\ \quad \cdot \dfrac{a_1 (X_{o2} - X_0) + b_1 (Y_{o2} - Y_0) + c_1 (Z_{o2} - Z_0)}{a_3 (X_{o2} - X_0) + b_3 (Y_{o2} - Y_0) + c_3 (Z_{o2} - Z_0)} - \Delta \mathrm{x} \\ y_{02} = -f \\ \quad \cdot \dfrac{a_2 (X_{o2} - X_0) + b_2 (Y_{o2} - Y_0) + c_2 (Z_{o2} - Z_0)}{a_3 (X_{o2} - X_0) + b_3 (Y_{o2} - Y_0) + c_3 (Z_{o2} - Z_0)} - \Delta \mathrm{y} \end{cases} \tag{9}$$

where

$a_1 = \cos\varphi \cos\kappa - \sin\varphi \sin\omega \sin\kappa$;
$a_2 = -\cos\varphi \sin\kappa - \sin\varphi \sin\omega \cos\kappa$;
$a_3 = -\sin\varphi \cos\omega$;
$b_1 = \cos\omega \sin\kappa$;
$b_2 = \cos\omega \cos\kappa$;
$b_3 = -\sin\omega$;
$c_1 = \sin\varphi \cos\kappa + \cos\varphi \sin\omega \sin\kappa$;
$c_2 = -\sin\varphi \sin\kappa + \cos\varphi \sin\omega \cos\kappa$;
$c_3 = \cos\varphi \cos\omega$;

(X_0, Y_0, Z_0) is the coordinate of the photographic center corresponding to the image plane; f, φ, ω, κ Δx and Δy are the parameter obtained by camera calibration.

Definition 3: Camera optical distortion model.

As the optical lens of measuring camera inevitably suffers from processing and assembly errors in the production process, the photographs taken by measuring camera must inevitably produce optical distortion in theory [11], [12]. Optical distortion will seriously interfere with the accuracy of the photogrammetric system. Therefore, in order to improve the accuracy of the photogrammetric measurement results, the optical distortion of the measuring camera must be corrected.

According to the research of RICOLFE-VIALA C [13]–[17], the camera optical distortion model, that is, the offset of image point in image plane coordinate system caused by optical distortion is shown in formula 10 and formula 11 at the bottom of the next page.

where

δ_x, δ_y, are the value of the results of the non-linear distortion synthesis in the x-axis and y-axis direction of the image plane coordinate system respectively;

$$QDYD = \sum_{\varepsilon=1}^{i-1} QL_g \cdot \left(\begin{array}{l} \left\{ X_o - \left[m_g \cdot \dfrac{m_g \cdot (X_o - X_g) + n_g \cdot (Y_o - Y_g) + p_g \cdot (Z_o - Z_g)}{m_g^2 + n_g^2 + p_g^2} + X_g \right] \right\}^2 \\ + \left\{ Y_o - \left[n_g \cdot \dfrac{m_g \cdot (X_o - X_g) + n_g \cdot (Y_o - Y_g) + p_g \cdot (Z_o - Z_g)}{m_g^2 + n_g^2 + p_g^2} + Y_g \right] \right\}^2 \\ + \left\{ Z_o - \left[p_g \cdot \dfrac{m_g \cdot (X_o - X_g) + n_g \cdot (Y_o - Y_g) + p_g \cdot (Z_o - Z_g)}{m_g^2 + n_g^2 + p_g^2} + Z_g \right] \right\}^2 \end{array} \right)^{\frac{1}{2}} \tag{8}$$

δ_{jx}, δ_{jy} are the radial distortion parameter in the direction of x-axis and y-axis in the image plane coordinate system respectively;

δ_{lx}, δ_{ly} are the eccentric distortion parameter in the direction of x-axis and y-axis in the image plane coordinate system respectively;

δ_{bx}, δ_{by} are the thin prism distortion parameters in the direction of x-axis and y-axis in the image plane coordinate system respectively;

k_1, k_2 is the radial distortion parameter;

q_1, q_2 are eccentric distortion parameters;

S_1, S_2 are the distortion parameters of the thin prism.

Due to the high cost of accurate camera calibration, the port front line does not have the conditions for accurate calibration of camera distortion parameters due to the pressure of cost control, and the approximate values of the relevant parameters can only be measured by a simple calibration method. Therefore, the effect of error correction directly based on optical distortion model is not obvious. However, the δ_x, δ_y calculated according to the parameters obtained by simple calibration method can intuitively and quantitatively reflect the size of position deviation of image points caused by optical distortion of lens to a certain extent.

In this paper, these parameters will be given a new function: calculating weights [18].

As shown in Fig. 7, according to the algorithm described in Section qdyd calculation method of weight coefficient, the image plane coordinate (x_A, y_A) of point A can be calculated from the image plane coordinate (x_a, y_a) of point a, as shown in formula 12 and formula 13 at the bottom of the page.

Based on the same principle, the image plane coordinate (x_B, y_B) of point B can be calculated from the image plane coordinate (x_b, y_b) of point b.

In Fig. 7, since the image point offsets $|\overrightarrow{aA}|$ and $|\overrightarrow{Bb}|$ caused by optical distortion are very small relative to the distance $|\overrightarrow{AB}|$ between point A and point B and the distance $|\overrightarrow{ab}|$ between point a and point b, it can be approximately considered that the straight line $l_{H_1o_1}$ passes through point h_1, and $\left|\overrightarrow{H_1o_1}\right| \approx \left|\overrightarrow{H_1o_2}\right| \approx \left|\overrightarrow{h_1o_2}\right|$. According to this principle, the calculation model for weight coefficient QDYD in Fig. 7 can be transformed into the simplified calculation model for weight coefficient QDYD shown in Fig. 8.

Based on the calculated coordinates of each point and the simplified calculation model for weight coefficient QDYD,

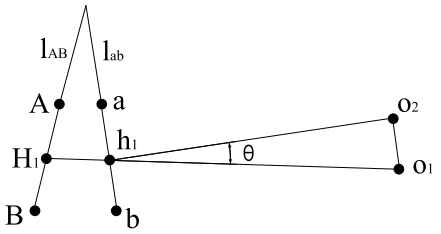

FIGURE 8. Schematic diagram of simplified calculation model for weight coefficient QDYD.

the distance calculation formula of point o_1 and point o_2 is shown in formula 14.

$$\left|\overrightarrow{o_1o_2}\right| = 2 \cdot \left|\overrightarrow{h_1o_2}\right| \cdot \sin\left[\frac{1}{2} \cdot \arccos\left(\frac{\overrightarrow{H_1h_1} \cdot \overrightarrow{h_1O_2}}{\left|\overrightarrow{H_1h_1}\right| \cdot \left|\overrightarrow{h_1o_2}\right|}\right)\right] \tag{14}$$

Set: According to the position of each point group on each measurement photo, $\left|\overrightarrow{o_1o_2}\right|$ calculated according to formula 14 is DOO_{gt}, $t = 1, 2, \ldots, p$, and p is the number of measurement photos.

After normalization, the calculation formula of the weight coefficient q of each perpendicular bisector is:

According to the algorithm described in formula 15, the weighted circle center-vertical foot distance solution model QDYD described in Definition 2 can be completed.

The weighted circle center-vertical foot distance solution model DYD in the equal weight radius prediction algorithm of rotary body structure is replaced by QL_g, which is the weighted radius prediction algorithm of rotary body structure.

D. ITERATIVE ALGORITHM FOR WEIGHTED PREDICTION OF RADIUS OF ROTARY BODY

The object coordinate of the predicted circle center o is derived from the result of equal weight circle center prediction. If the center result of the weighted prediction algorithm of radius of rotary body is used as the solution basis and iterative operation is carried out, the iterative algorithm for weighted prediction of radius of rotary body as shown in Fig. 9 can be formed. The purpose of setting up this algorithm includes:

1. The accuracy of the measurement results of the weighted prediction algorithm of radius of rotary body is further optimized;

$$\delta_x = \delta_{jx} + \delta_{lx} + \delta_{bx} = k_1 x\left(x^2 + y^2\right) + \left[q_1\left(3x^2 + y^2\right) + 2q_2xy\right] + s_1\left(x^2 + y^2\right) \tag{10}$$

$$\delta_y = \delta_{jy} + \delta_{ly} + \delta_{by} = k_2 y\left(x^2 + y^2\right) + \left[q_2\left(3x^2 + y^2\right) + 2q_1xy\right] + s_2\left(x^2 + y^2\right) \tag{11}$$

$$x_A = x_a - \left\{k_1x_a\left(x_a^2 + y_a^2\right) + \left[q_1\left(3x_a^2 + y_a^2\right) + 2q_2x_ay_a\right] + s_1\left(x_a^2 + y_a^2\right)\right\} \tag{12}$$

$$y_A = y_a - \left\{k_2y_a\left(x_a^2 + y_a^2\right) + \left[q_2\left(3x_a^2 + y_a^2\right) + 2q_1x_ay_a\right] + s_2\left(x_a^2 + y_a^2\right)\right\} \tag{13}$$

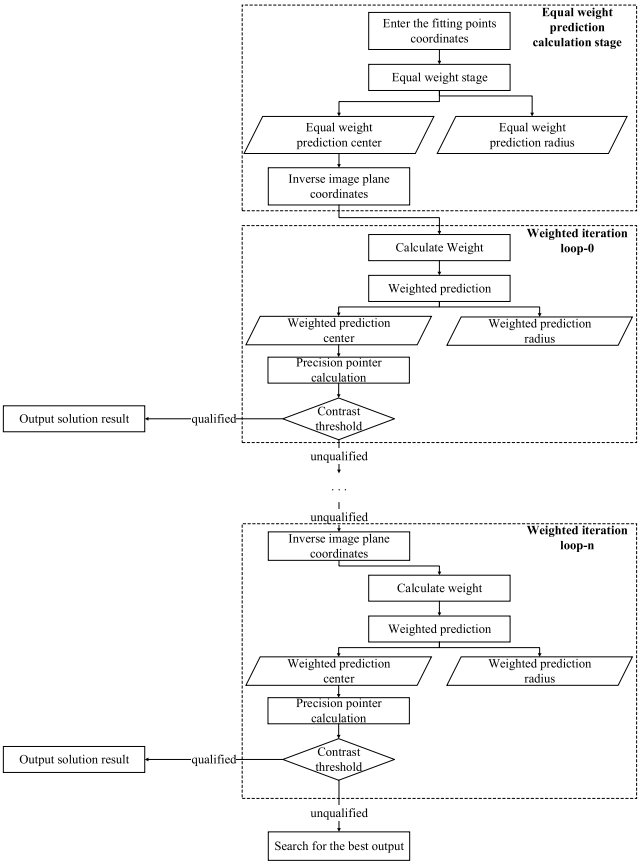

FIGURE 9. Flow chart of iterative algorithm for weighted prediction of radius of rotary body.

2. While improving the accuracy of measurement results, it also balances the execution efficiency of the algorithm.

In order to achieve the above objectives, a decision threshold YZ_{RD} should be set for the weighted circle center-vertical foot distance solution model QDYD, which can quantify the accuracy of the calculation results. If the following conditions are met, the accuracy of the solution results can be considered as meeting the requirements, then the iteration can be terminated and the results can be output.

As shown in Fig. 9, the maximum number of iterations n can be set during the actual measurement process. When the number of iterations reaches the upper limit and the measurement result still does not meet the criterion of formula 16, as shown at the bottom of the page, the iteration data corresponding to the minimum value of the weighted circle center-vertical foot distance solution model QDYD can be output as the solution result.

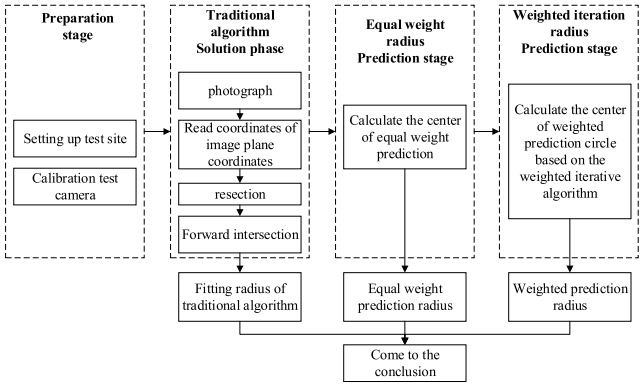

FIGURE 10. Verification test step diagram.

$$QL_g = \frac{\left(\sum_{t=1}^{p} DOO_{gt}\right)^{-1}}{\sum_{g=1}^{i-1}\left(\sum_{t=1}^{p} DOO_{gt}\right)^{-1}} \tag{15}$$

III. CASE STUDY

In order to verify the actual accuracy correction effect of the algorithm described in Section II, this paper designed the verification test as shown in Fig. 10. The procedure of this test is as follows:

1. Preparatory phase: In this stage, a test fields will be built for principle verification model and engineering test prototype respectively, and test photos will be collected. In addition, in this stage, the existing simple calibration method and the patent method held by the author will be used to complete the calibration of the internal parameter matrix of the test camera;

2. Traditional algorithm solution stage: According to the forward intersection solution results of the classical photogrammetric method [19] the traditional algorithm [20]–[22] was used to solve the fitting radius of the test object based on the fitting principle of space circle;

3. Equal weight radius prediction stage: Solve the equal weight prediction radius according to the prediction

$$\sum_{g=1}^{i-1} QL_g \cdot \left(\begin{array}{l} \left\{ X_o - \left[m_g \cdot \dfrac{m_g \cdot (X_o - X_g) + n_g \cdot (Y_o - Y_g) + p_g \cdot (Z_o - Z_g)}{m_g^2 + n_g^2 + p_g^2} + X_g \right] \right\}^2 \\ + \left\{ Y_o - \left[n_g \cdot \dfrac{m_g \cdot (X_o - X_g) + n_g \cdot (Y_o - Y_g) + p_g \cdot (Z_o - Z_g)}{m_g^2 + {n_g}^2 + {p_g}^2} + Y_g \right] \right\}^2 \\ + \left\{ Z_o - \left[p_g \cdot \dfrac{m_g \cdot (X_o - X_g) + n_g \cdot (Y_o - Y_g) + p_g \cdot (Z_o - Z_g)}{{m_g}^2 + n_g^2 + {p_g}^2} + Z_g \right] \right\}^2 \end{array} \right)^{\frac{1}{2}} \leq YZ_{RD} \tag{16}$$

algorithm of prediction radius of rotary body described in Section equal weight radius prediction of rotary body structure;

4. Weighted radius prediction stage: Based on the calculation results of equal weight radius prediction stage, the weighted prediction radius is calculated according to the weighted prediction iteration algorithm of rotary body radius described in Section iterative algorithm for weighted prediction of radius of rotary body.

By comparing the measurement errors of the traditional algorithm's fitting radius, the equal-weight prediction radius and the weighted prediction radius, the correction effect of the algorithm described in this paper can be scientifically evaluated.

In addition, in order to fully test the theoretical execution effect of the algorithm and the actual engineering application effect, according to the test step shown in Fig. 10, this paper sets two sets of parallel tests for different test objects:

1. Principle verification test:

Based on the principle verification model, the experiment is carried out in the laboratory to verify the implementation effect of the algorithm in the ideal state;

2. Simulation engineering test:

Based on the engineering verification prototype, the test is carried out in the outdoor test field to verify the real application effect of the algorithm proposed in this paper when measuring the large-scale port hoisting machinery in the actual engineering application environment.

A. PREPARATION STAGE

1) SET UP THE TEST SITE

The test field used in the principle verification test is shown in Fig. 11. Combined with the port hoisting machinery and the algorithm characteristics described in this paper, the principle verification model has the following characteristics:

1. It has the characteristic structure of the revolving body, and there are a certain number of feature points on the edge of the revolving body, which can be used to simulate the circumferential structure characteristics of the slewing mechanism in the measurement operation scene of port hoisting machinery such as stiffeners, gear tooth rings, etc;

2. The control points are set on a structure composed of standard size squares, making the object square coordinates easy to read;

3. The size of the revolving body used in the experiment is accurate due to strict inspection and calibration. In this paper, the radius of the small cylinder at the top is used to provide support for the scientific measurement of the accuracy of the algorithm.

In Fig. 11, points 1 to 4 are control points; point *a* and point *b* are the intensive reading pointer point, these two points, together with the patented algorithm proposed by the author, can achieve the precise calibration of focal length; Points *A* to *D* are the test points, and they will be used to calculate the radius of the rotary body.

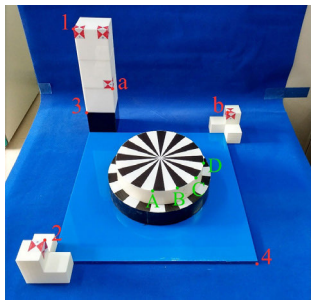

FIGURE 11. Schematic diagram of the principle verification model test site.

TABLE 1. Coordinate of the object space of control point and test point of verification test B.

Point	x(mm)	y(mm)	z(mm)
1	0	0	400
2	500	0	100
3	0	0	100
4	500	500	0
a	0	100	200
b	0	500	100

In coordinate system of the object space, the object square coordinates of each calibration point and the intensive reading pointer point in the model test field of the principle verification model can be read directly, because the precise shape dimensions of calibration block and test model are known.

The object square coordinates of each point are shown in Table 1:

The test fields used for simulated engineering tests are shown in Fig. 12. In order to be as close as possible to the actual engineering, a portal crane model located in School of Logistics Engineering of Wuhan University of Technology is selected as the engineering test prototype in this test. According to the test report issued by the Port Logistics Technology and Equipment Engineering Research Center of the Ministry of Education of the People's Republic of China, the diameter of the seat circle of the slewing mechanism of this equipment is RD = 1100 (mm).

Similar to the test point setting principle of the principle verification model, the test point setting scheme of the engineering test prototype test field is shown in Fig. 12. In this experiment, points 1 to 4 are the control points; points *a*, *b* are intensive reading pointer point. In this test, four test points, such as a bit DA- point DD, are set up to fit the seat ring diameter RD.

In coordinate system of the object space, the coordinate values of each calibration point and intensive reading pointer point of the engineering test prototype test site are measured by total station. The measurement site is shown in Fig. 13.

a. Selection scheme of control points and pointer points

b. Selection Scheme for Test Points

FIGURE 12. Schematic diagram of test site for engineering test prototype.

FIGURE 13. Calibration site of engineering test prototype.

TABLE 2. Object square coordinates of control point and pointer point of test object B.

Point	x(mm)	y(mm)	z(mm)
1	-7807	-2699	3034
2	-15013	-3492	-550
3	-10173	-5315	610
4	-8413	1431	-125
a	-10037	-1219	1488
b	-8446	163	-161

In Fig. 12, the object square coordinates of each point are shown in Table 2:

2) CALIBRATION TEST CAMERA

The camera used in this experiment was a Canon EOS 5Ds. The technical parameters of this camera are shown in Table 3. In order to ensure the relative stability of the focal length f and the clarity of the photos used for calculation during the test, when taking the photos used for calibration and the test photos, the method of using automatic focusing mode (AF) to complete the focusing at the nearest measuring station and then switching to manual focusing mode (MF) to complete the shooting is adopted.

The camera calibration tool used in this experiment is MATLAB Camera Calibrator toolbox., which is a mature camera calibration tool widely used for accurate results and convenient establishment of calibration field. The calibration results of the camera are shown in Table 4.

In the table: Δx, Δy is the deviation of the center of the image plane coordinate system; k_1, k_2 is the radial distortion parameter of the camera; q_1, q_2 is the eccentricity distortion parameter of the camera; s_1, s_2 is the thin prism distortion of the camera.

TABLE 3. Test camera parameters.

Parameter name	Parameter value	Unit
The resolution of the CCD	8688*5792	(pixel)
Single pixel size	4.14	(μ m)

TABLE 4. Calibration results of the test camera.

Parameter	Numerical value
△x(mm)	-0.0787
△y(mm)	-0.1242
k1	-0.1097
k2	-0.0137
q1	0
q2	0
s1	0
s2	0

TABLE 5. Camera calibration parameters based on test methods.

Parameter	Numerical value
f1(mm)	57.30
f2(mm)	65.32

Because of the large difference in the shooting distance between the principle verification model test ground and the engineering test prototype test ground, the actual shooting focal length of the principle verification model and the engineering test prototype will be different due to the automatic focusing operation of the camera in the actual shooting process. The existing differences are calibrated by the patent algorithm, which is held by the author of this paper. Detailed values are shown in Table 5. In the table: $f1, f2$ are the focal length calibration values of the principle verification test and the simulation engineering test respectively.

B. TRADITIONAL ALGORITHM SOLVING STAGE

1) SELECTION OF PHOTOGRAPHIC POINTS

a: PHOTO SELECTION DATA OF THE PRINCIPLE VERIFICATION TEST

In this paper, two photos are used to solve the problem. According to the customary appellation of the traditional

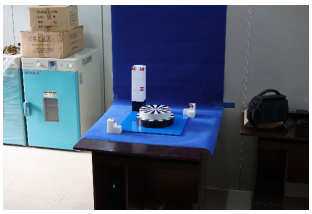

FIGURE 14. Left photo of principle verification test.

FIGURE 15. Right photo of principle verification test.

TABLE 6. Artificial identification results of test control points, precision pointer points, test points of principle verification test.

Point	x-left(mm)	y-left(mm)	x-right(mm)	y-right(mm)
1	-4.738	-2.834	-3.650	1.140
2	1.327	-4.809	1.543	-4.641
3	-0.741	-2.831	0.308	1.056
4	3.363	2.846	5.048	-0.074
a	-1.965	-1.502	-0.700	1.963
b	-0.335	3.898	1.963	5.803
A	0.704	-0.711	1.790	-1.004
B	0.718	0.260	1.994	-0.305
C	0.606	1.139	2.084	0.641
D	0.396	1.680	2.031	1.581

algorithm, these are named left photo and right photo respectively. The left and right photos collected in the principle verification test are shown in Fig. 14 and Fig. 15 respectively.

In order to show the precision optimization effect of the algorithm described in this paper as clearly as possible, the coordinates of each control point, precision pointer point and test point in the image plane coordinate system are obtained by manual selection. The detailed parameters of the selection point are shown in Table 6.

b: PHOTO SELECTION DATA OF SIMULATED ENGINEERING TEST

Similar to the process of the principle verification test, the test photos collected from the simulation engineering test are

FIGURE 16. Left photo of the simulated engineering test.

FIGURE 17. Right photo of the simulated engineering test.

TABLE 7. Artificial identification results of control points, precision pointer points and test points in simulated engineering tests.

Point	x-left(mm)	y-left(mm)	x-right(mm)	y-right(mm)
1	-3.874	8.102	-10.270	2.575
2	9.452	2.251	4.764	6.320
3	6.039	12.778	0.970	13.251
4	8.519	-8.677	3.697	-14.229
a	2.763	0.155	-2.330	-2.313
b	8.685	-3.501	3.898	-9.181
DA	-1.038	-1.887	-6.229	-3.972
DB	-1.174	-0.845	-6.459	-3.341
DC	-1.177	0.440	-6.574	-2.122
DD	-1.035	1.536	-6.506	-0.697

shown in Fig. 16 and Fig. 17. The image plane coordinates obtained by manual selection are shown in Table 7.

2) SOLUTION RESULTS OF CLASSIC ALGORITHMS

In this test, the method described in Analytical Photogrammetry [19], written by Academician Deren Li of Wuhan University, is used to calculate the object coordinates of each test point. This method is the most widely used algorithm in the field of photogrammetry at present. After calculation based on this method, the calculation results are as follows:

a: SOLUTION RESULTS OF CLASSICAL ALGORITHM OF PRINCIPLE VERIFICATION TEST

1. The exterior orientation parameters of the left and right photos of the principle verification test are shown in Table 8:

TABLE 8. Calculation results of exterior orientation parameters in principle verification test.

	left photo	right photo
X	3597.183(mm)	2381.019(mm)
Y	958.450(mm)	2861.613(mm)
Z	1146.403(mm)	1169.353(mm)
ψ	-1.277(rad)	-1.148(rad)
ω	-0.196(rad)	-0.852(rad)
κ	0.066(rad)	0.339(rad)

TABLE 9. Calculation results of classical photogrammetry algorithm in principle verification test.

Point	X(mm)	Y(mm)	Z(mm)
A	375.597	242.177	120.479
B	366.734	305.473	121.220
C	329.620	357.197	121.396
D	272.173	383.259	120.688

TABLE 10. Calculation results of classical space circle fitting algorithm.

O			R(mm)
X(mm)	Y(mm)	Z(mm)	133.268
243.050	255.910	118.758	

2. The object square coordinates of each test point in the principle verification test are calculated by classical photogrammetry, as shown in Table 9:

3. The object square coordinate and radius of the center of the circle calculated based on the classical spatial circle fitting algorithm are shown in Table 10.

b: CLASSICAL ALGORITHM SOLUTION OF SIMULATION ENGINEERING TEST

1. The exterior orientation parameters of the simulation engineering test are shown in Table 11.

2. The object square coordinates of each test point in the simulation engineering test calculated by classical photogrammetry are shown in Table 12.

3. According to the data in Table 12, the object square coordinate and radius of the center of the circle calculated based on the classical spatial circle fitting algorithm are shown in Table 13.

TABLE 11. Calculation results of exterior orientation parameters in simulation engineering test.

Point	Left photo	Right photo
X	7568.682(mm)	6976.212(mm)
Y	3905.267(mm)	-3626.244(mm)
Z	103.411(mm)	12.754 (mm)
ψ	26.583(rad)	1.523(rad)
ω	0.281(rad)	-0.102(rad)
κ	31.458(rad)	6.281(rad)

TABLE 12. Calculation results of classical photogrammetric algorithm in simulated engineering test.

Point	X(mm)	Y(mm)	Z(mm)
A	-10400.654	-755.008	2543.097
B	-10083.550	-976.414	2554.393
C	-9961.301	-1319.239	2559.310
D	-10082.725	-1682.518	2552.704

TABLE 13. Calculation results of classical space circle fitting algorithm.

O			R (mm)
X(mm)	Y(mm)	Z(mm)	616.589
-10576.961	-1345.835	2538.375	

TABLE 14. Calculation results of equal weight space circle fitting algorithm.

O			R (mm)
X(mm)	Y(mm)	Z(mm)	123.642
248.828	257.813	118.378	

C. EQUAL WEIGHT RADIUS PREDICTION STAGE

1) EQUAL WEIGHT RADIUS PREDICTION OF PRINCIPLE VERIFICATION TEST

According to the data in Table 9 and the prediction algorithm of the radius of the rotating body with equal weight described in Section Equal weight radius prediction of rotary body structure, the object square coordinate of O_d and radius R_d of the circle obtained can be calculated. Specific values are shown in Table 14:

TABLE 15. Calculation results of equal weight space circle fitting algorithm.

O			R (mm)
X(mm)	Y(mm)	Z(mm)	616.589
-10576.961	-1345.835	2538.375	

TABLE 16. Iteration weight of validation test B.

Iteration steps	Q1	Q2	Q3
loop1	0.099094	0.693170	0.207736
loop2	0.098069	0.693934	0.207997
loop3	0.098060	0.693914	0.208026

TABLE 17. Iteration results of validation test B.

Iteration	O			R (mm)
steps	X(mm)	Y(mm)	Z(mm)	
loop1	249.388	259.627	118.417	123.396
loop2	249.405	259.644	118.922	123.478
loop3	249.533	259.732	119.118	123.886

2) EQUAL WEIGHT RADIUS PREDICTION OF SIMULATION ENGINEERING TEST

According to the data in Table 12 and the prediction algorithm of the radius of the rotating body with equal weight described in Section Equal weight radius prediction of rotary body structure, the object square coordinate of O_d and radius R_d of the circle obtained can be calculated. Specific values are shown in Table 15

D. WEIGHTED RADIUS PREDICTION STAGE

The termination threshold set in the principle verification test and simulation engineering test of this paper is 4 (mm), and the maximum number of iteration steps is 10 (step).

1) WEIGHTED RADIUS PREDICTION OF PRINCIPLE VERIFICATION TEST

Three iterations were carried out in the principle verification test, and the weights Q_1, Q_2, Q_3 of each perpendicular bisector in each iteration are shown in Table 16.

In the principle verification test, the object square coordinate value O_q of the weighted prediction center and the radius value R_q of the weighted prediction obtained in each iteration are shown in Table 17. The measurement result corresponding to loop 3 is the final calculation result of verification test B.

TABLE 18. Iteration weight of validation test B.

Iteration steps	Q_1	Q_2	Q_3
loop1	0.1721942	0.4725261	0.3552796
loop2	0.1712563	0.4707216	0.3580219
loop3	0.1712618	0.4708164	0.3579217

TABLE 19. Iteration results of validation test B.

Iteration	O			R (mm)
steps	X(mm)	Y(mm)	Z(mm)	
loop1	-10550.888	-1329.435	2535.254	557.618
loop2	-10550.820	-1329.401	2535.258	557.554
loop3	-10550.820	-1329.402	2535.257	557.556

TABLE 20. Error comparison of measurement results of principle verification test.

	Classical algorithm	equal weight algorithm	weighted algorithm
Measured value (mm)	133.268	122.642	123.886
Measurement error (mm) (Absolute value)	8.268	2.358	1.114
Relative error (Absolute value)	6.614%.	1.886%	0.891%

2) WEIGHTED RADIUS PREDICTION OF SIMULATED ENGINEERING TEST

Three iterations were carried out in the simulation engineering test, and the weights Q_1, Q_2, Q_3 of each perpendicular bisector in each iteration are shown in Table 18.

In the principle verification test, the object square coordinate value O_q of the weighted prediction center and the radius value R_q of the weighted prediction obtained in each iteration are shown in Table 17. The measurement result corresponding to loop 3 is the final calculation result of verification test B.

IV. RESULTS AND DISCUSSION

The errors of measurement results of principle verification test and the errors of measurement results of classical algorithm, equal weight algorithm and weighted algorithm in simulation engineering test are shown in Table 20 and Table 21 respectively.

The error comparison between the calculation results in each stage of the principle verification test and the simulation engineering test is shown in Fig. 18 and Fig. 19.

From the above comparison data, it can be seen that the errors of settlement results of traditional algorithm,

TABLE 21. Error comparison of measurement results of simulation engineering test.

	Classical algorithm	equal weight algorithm	weighted algorithm
Measured value (mm)	616.589	562.348	557.556
Measurement error (mm) (Absolute value)	66.589	12.348	7.556
Relative error (Absolute value)	12.107%	2.245%	1.374%

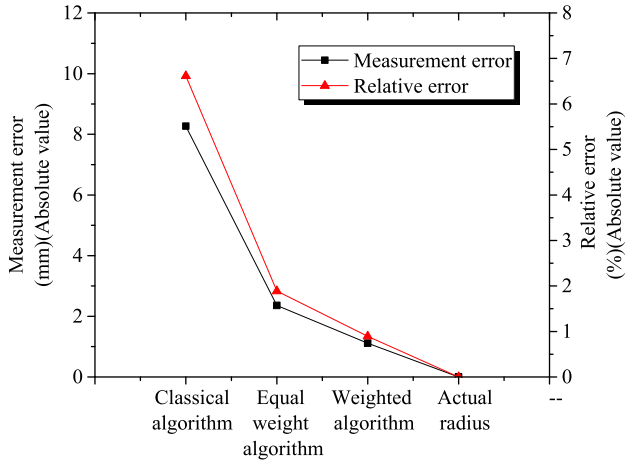

FIGURE 18. Comparison diagram of error in principle verification test.

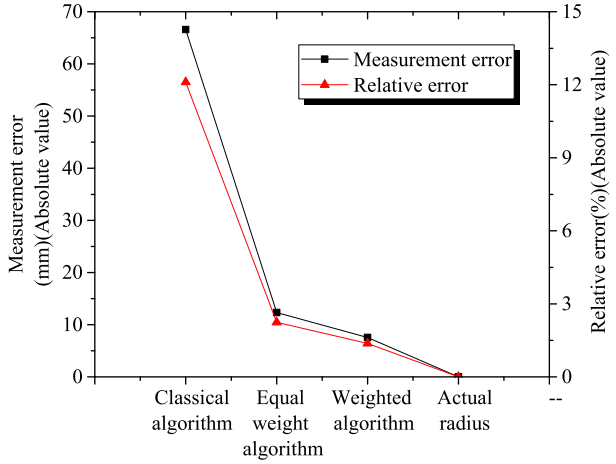

FIGURE 19. Comparison diagram of error in simulated engineering test.

equal weight algorithm and weighted algorithm decreases gradually, and the correction range is large. This shows that, compared with the traditional algorithm, the weighted radius prediction iterative optimization algorithm proposed in this paper can significantly improve the accuracy of the radius fitting results when the data volume is used to fit fewer circle points. This is of great significance for the measurement of the rotary body structure of the port hoisting machinery with limited characteristic points and inconvenient manual sticking.

V. CONCLUSION

Based on the optical distortion model and through the simplified model described in chapter 2.3.2, the quantitative confidence assessment of fitting data based on lens optical distortion model is realized, and the weighted fitting method of measuring data of center and radius is proposed based on this theoretical basis. In order to balance the accuracy of measurement results and the execution efficiency of the algorithm, this paper also proposes the iterative algorithm described in Chapter 2.4. Experiments show that the method proposed in this paper can significantly improve the accuracy of measurement results when the fitting data is limited. It is of great significance to the measurement of large-scale mechanical rotary body structure represented by port hoisting machinery, with limited data of surface feature points and inconvenient to set up manual mark points. However, during the experiment, the setting of relevant iteration parameters still comes from the operating experience of scientific researchers, which not only has a negative impact on the optimization of measurement results accuracy, but also hinders the promotion of the algorithm in this paper. In the subsequent research, the author and members of the scientific research team will use machine learning method to explore the two variables of the size level of the measured object and the distance between the measuring station and the measured object, and study their influence mechanism on the optimal setting scheme of the iterative parameters in the iteration method described in this paper. In this way, an automatic setting scheme of relevant parameters is proposed, which further improves the accuracy of measurement results and the ease of use of the algorithm.

ACKNOWLEDGMENT

The authors express their sincere gratitude to the journal's editor and anonymous reviewers for their help in revising the paper.

AUTHOR CONTRIBUTIONS

Enshun Lu and Yang Liu built the mathematical model and developed the general methodological framework. As the first author Enshun Lu performed the research, analyzed the data, discussed the results and wrote this research article. Yang Liu is the corresponding author of this paper. All authors have read and approved the final manuscript.

REFERENCES

[1] L. B. Zhu, X. Wu, and H. Chen, "Study on special equipment safety risk assessment and control measures," (in Chinese), *China Saf. Sci. J.*, vol. 24, no. 1, pp. 149–155, 2014.

[2] AQSIQ. *A Report on the National Safety Status of Special Equipment in 2015*. Accessed: Jan. 17, 2017. [Online]. Available: http://www.aqxx.org/Item/103703.aspx

[3] S. Ruud and Å. Mikkelsen, "Risk-based rules for crane safety systems," *Rel. Eng. Syst. Saf.*, vol. 93, no. 9, pp. 1369–1376, Sep. 2008.

[4] O. N. Aneziris, I. A. Papazoglou, M. L. Mud, M. Damen, J. Kuiper, H. Baksteen, B. J. Ale, L. J. Bellamy, A. R. Hale, A. Bloemhoff, J. G. Post, and J. Oh, "Towards risk assessment for crane activities," *Saf. Sci.*, vol. 46, no. 6, pp. 872–884, Jul. 2008.
[5] A. Li and Z. Zhao, "Crane safety assessment method based on entropy and cumulative prospect theory," *Entropy*, vol. 19, no. 1, p. 44, Jan. 2017.
[6] A. Li and Z. Zhao, "An improved model of variable fuzzy sets with normal membership function for crane safety evaluation," *Math. Problems Eng.*, vol. 2017, no. 1, pp. 1–13, 2017.
[7] Q. Wang, Z. Zhao, E. Lu, Y. Liu, and L. Liu, "A robust and accurate camera pose determination method based on geometric optimization search using Internet of Things," *Int. J. Distrib. Sensor Netw.*, vol. 15, no. 6, Jun. 2019, Art. no. 155014771985758.
[8] E. Lu, Z. Zhao, Q. Wang, Y. Liu, and L. Liu, "A weighting intersection point prediction iteration optimization algorithm used in photogrammetry for port hoisting machinery," *Opt. Laser Technol.*, vol. 111, pp. 323–330, Apr. 2019.
[9] A. Li, Z. Zhao, and M. Wen, "Multiple attribute decision making with completely unknown weights based on cumulative prospect theory and grey system theory," in *Proc. Int. Conf. Intell. Inf. Process.*, 2016, pp. 1–7.
[10] C. Wohlin *et al.*, *Experimentation in Software Engineering*. Norwell, MA, USA: Kluwer, 1999.
[11] C. Ricolfe-Viala and A.-J. Sánchez-Salmerón, "Using the camera pin-hole model restrictions to calibrate the lens distortion model," *Opt. Laser Technol.*, vol. 43, no. 6, pp. 996–1005, Sep. 2011.
[12] J. Weng, P. Cohen, and M. Herniou, "Camera calibration with distortion models and accuracy evaluation," *IEEE Trans. Pattern Anal. Mach. Intell.*, vol. 14, no. 10, pp. 965–980, Oct. 1992.
[13] J. Dazhi, Q. Yu, and B. Wang, "Research and overview of imaging non-linear distortion in computer vision," *Comput. Eng.*, vol. 27, no. 12, pp. 108–110, 2001.
[14] J. Dazhi, Q. Yu, J. Sun, and Q. Ding, "Research on solving nonlinear distortion of camera lens by a standard graphic method," *J. Southeast Univ., Nat. Sci. Ed.*, vol. 31, no. 4, pp. 111–116, 2001.
[15] C. Ricolfe-Viala and A.-J. Sánchez-Salmerón, "Correcting non-linear lens distortion in cameras without using a model," *Opt. Laser Technol.*, vol. 42, no. 4, pp. 628–639, Jun. 2010.
[16] Z. Wang, H. Kieu, H. Nguyen, and M. Le, "Digital image correlation in experimental mechanics and image registration in computer vision: Similarities, differences and complements," *Opt. Lasers Eng.*, vol. 65, pp. 18–27, Feb. 2015.
[17] P. Zhao, *The Research and Development of Machine Vision*. Beijing, China: Mammalia Science Press, 2012.
[18] B. Ren, G. Jin, Y. Zhang, X. Zhong, and L. Kong, "Influence of image motion on TDI imaging camera by distortion effect," (in Chinese), *Infr. Laser Eng.*, vol. 43, no. 12, pp. 3951–3957, 2014.
[19] D. Li *et al.*, in *Proc. 8th Int. Symp. Spatial Accuracy Assessment Natural Resour. Environ. Sci.*, Shanghai, China, Jun. 2008.
[20] A. Fitzgibbon, M. Pilu, and R. B. Fisher, "Direct least square fitting of ellipses," *IEEE Trans. Pattern Anal. Mach. Intell.*, vol. 21, no. 5, pp. 476–480, May 1999.
[21] Z. Yongjun, "Reconstruction of circles and round rectangles by generalized point photogrammetry," *J. Harbin Inst. Technol.*, vol. 40, no. 1, pp. 136–140, 2008.
[22] J. Zhang, M. Sun, S. Zheng, and Z. Ji, "3D reconstruction of a Yuan dynasty blue-and-white porcelain based on profile constraint and photogrammetry," *Geomatics Inf. Sci. Wuhan Univ.*, vol. 34, no. 1, pp. 7–10, 2009.

ENSHUN LU received the B.S. degree in mechanical engineering from the Wuhan Huaxia University of Technology, Wuhan, China, in 2013, and the M.S. and Ph.D. degrees in mechanical engineering from the Wuhan University of Technology, Wuhan, in 2016 and 2019, respectively. He is currently a Postdoctoral Researcher with the School of Energy and Power Engineering, Wuhan University of Technology. His research interests include computer vision measurement, and close range photogrammetry and measurement of large engineering equipment.

YANG LIU received the B.S. degree in fundamental mathematics and the M.S. and Ph.D. degrees in computational mathematics from the Wuhan University, Wuhan, China, in 2001, 2004, and 2014, respectively. He is currently an Associate Professor with the School of Science, Wuhan University of Technology, Wuhan. His research interests include computational mathematics and application of mathematics to engineering.

ZHANGYAN ZHAO received the B.S. degree in mechanical engineering from Southwest Jiaotong University, Chengdu, China, in 1985, and the M.S. and Ph.D. degrees in mechanical engineering from the Wuhan University of Technology, Wuhan, China, in 1991 and 2001, respectively. He is currently a Professor and a Doctoral Supervisor with the School of Logistics Engineering, Wuhan University of Technology. He has authored three books and published over 100 prestigious journal papers and conference papers. He holds six patents. His research interests include metal structure fault diagnosis and safety evaluation, computer vision measurement, and computer-aided engineering and manufacturing.

YIFAN LIU received the B.S. and M.S. degrees in mechanical engineering, Wuhan, China, in 2018 and 2020, respectively. She is currently working as a Designer at China harzone Industry Corporation Ltd. Her research interests include measurement of large engineering equipment and mechanical design and manufacturing.

CHENGHUA ZHANG received the B.S. degree in mechanical design and manufacturing and automation from the North China University of Science and Technology, Tangshan, China, in 2016, and the M.S. degree in mechanical engineering from the Wuhan University of Technology, Wuhan, China, in 2018, where he is currently pursuing the Ph.D. degree. His research is based within the School of Logistics Engineering under the supervision of Prof. Zhao. His research interests include computer vision measurement, and close range photogrammetry and measurement of large engineering equipment.